

# Theory and experiments of disorder-induced resonance shifts and mode-edge broadening in deliberately disordered photonic crystal waveguides

Nishan Mann,<sup>1,\*</sup> Alisa Javadi,<sup>2</sup> P. D. García,<sup>2</sup> Peter Lodahl,<sup>2</sup> and Stephen Hughes<sup>1</sup>

<sup>1</sup>*Department of Physics, Queen's University, Kingston, Ontario, Canada, K7L 3N6*

<sup>2</sup>*Niels Bohr Institute, University of Copenhagen, Blegdamsvej 17, DK-2100 Copenhagen, Denmark*

(Received 13 May 2015; published 26 August 2015)

We study both theoretically and experimentally the effects of introducing deliberate disorder in a slow-light photonic crystal waveguide on the photon density of states. We introduce a theoretical model that includes both deliberate disorder through statistically moving the hole centers in the photonic crystal lattice and intrinsic disorder caused by fabrication imperfections. We demonstrate a disorder-induced mean blueshift and an overall broadening of the photonic density of states for deliberate disorder values ranging 0–12 nm. By comparing with measurements obtained from a GaAs photonic crystal waveguide, we find very good agreement between theory and experiment. These results highlight the importance of carefully including local field effects for modeling high-index contrast perturbations and demonstrate the efficiency of our perturbative approach for modeling disorder-induced changes in the density of states. Our work also demonstrates the importance of using asymmetric dielectric polarizabilities for positive and negative dielectric perturbations when modeling a perturbed dielectric interface in photonic crystal platforms. Finally, we also show examples of disorder-induced resonances that can appear for various instances of disorder.

DOI: [10.1103/PhysRevA.92.023849](https://doi.org/10.1103/PhysRevA.92.023849)

PACS number(s): 42.70.Qs, 42.25.Fx, 42.82.Et, 42.81.Dp

## I. INTRODUCTION

Photonic crystal (PC) cavities and waveguides are attractive nanophotonic platforms for controlling and studying fundamental light-matter interactions. Aided by the presence of a photonic band gap (PBG), which arises from the underlying periodic dielectric structure, light within a PC cavity or PC waveguide can be strongly confined within a small volume or area. In the case of a PC waveguide (PCW), light can be slowed down by orders of magnitude compared to a typical slab or ridge waveguide, which acts to increase the local density of photonic states (LDOS). The ability to control light-matter interactions in PC platforms leads to a host of photonic applications and rich optical interactions [1,2]. For example, PC cavities have been used for exploring cavity quantum electrodynamics (cavity-QED) in both the weak- and strong-coupling regimes [3,4], while PCWs have been exploited to realize on-chip single-photon sources [5–7]. Slow light in PCWs also enhances nonlinear processes including pulse compression and soliton propagation [8], third-harmonic generation [9], and four-wave mixing [10]. In addition, PCWs have been integrated in various photonic circuits, as optical sensor elements for refractive index measurements in biosensing [11], and chemical fluid detection [12].

In practice, PCWs are highly sensitive to fabrication imperfections (intrinsic disorder) which is inevitably introduced at the fabrication stage. Disorder-induced losses are particularly detrimental in the slow-light regime [13], which was predicted theoretically by Hughes *et al.* [14] using a photonic Green function approach and is now a common finding amongst various similar theoretical works in the literature [15–18]. With continued improvements in semiconductor fabrication techniques, and improved theoretical understanding about how

to mitigate disorder-induced losses [19,20], various groups have experimentally demonstrated PCW designs that have reduced disorder-induced losses [21,22].

However, disorder in PCs is not necessarily a hindrance as was noticed by John in 1987 [23], who proposed disordered PCs for experimentally observing the well-known phenomena of Anderson localization. Topolancik *et al.* [24] experimentally demonstrated spectral peaks bearing signatures of Anderson localization arising from localized modes in a deliberately disordered PCW. Patterson *et al.* [25] utilized coupled mode theory to highlight the effect of light localization via multiple scattering by examining the transmission through a PCW in the slow-light regime. The strong localized resonances in disordered PCWs have also been used to enhance the spontaneous emission factor of embedded quantum dots [26], and recently Thyrrstrup *et al.* [27] have proposed coupling quantum dot emitters to a disordered PCW as a promising platform for conducting QED experiments. Other applications of disordered PCWs include enhanced light harvesting and random lasing [28].

Apart from causing propagation losses and disorder-induced localized resonances, disorder also induces changes in the eigenfrequencies and eigenmodes of the underlying PC. Ramunno and Hughes [29] modeled disorder-induced resonance shifts in PC nanocavities and predicted a nontrivial disorder-induced mean blueshift in the cavity resonance. Patterson and Hughes [30] extended this formalism to PCWs, and predicted both a mean blueshift of resonances and a disorder-induced mode-edge broadening. To the best of our knowledge, this mean blueshift has not been experimentally measured; this is likely because no one has realized a simple experimental procedure for proving that a mean blueshift occurs, especially for an intrinsically disordered PCW. Both of the theoretical works mentioned above dealt with intrinsic disorder only, which occurs via rapid fluctuations of the air-dielectric interface and highlighted the importance of carefully taking into account local fields at the interface.

\*nmann@physics.queensu.ca

Recently, Savona has exploited a guided mode expansion technique to compute disorder-induced localized modes and the corresponding spectral density, which, as expected, yields sharp spectral signatures near the mode edge, indicative of spatially localized modes [31].

In this paper, we introduce an intuitive model to describe disorder-induced resonance shifts and broadening of the fundamental mode below the light line which takes into account a systematic increase of the disorder parameters (i.e., it allows one to model deliberate disorder which can be controlled and changed in a systematic way). We show how one can extend the theoretical models introduced in Refs. [29,30] to account for both intrinsic and deliberate or extrinsic disorder where extrinsic disorder is characterized by a deliberate shift of the hole centers. Denoting the first-order perturbative correction to the eigenfrequencies of the fundamental waveguide mode as  $\Delta\omega$ , we carefully include local field effects [32] in our model to compute the mean ( $\mathbb{E}[\Delta\omega]$ ) and the quadratic mean (rms) ( $\sqrt{\mathbb{E}[\Delta\omega^2]}$ ) of the first-order correction term, where  $\mathbb{E}[\cdot]$  denotes the expectation. As a result, we find that on average, the band structure including the mode edge is broadened and blueshifted, causing the DOS to shift above the nominal mode edge. For disordered PCWs with varying extrinsic disorder (see Ref. [33] for details), we then compute the ensemble averaged DOS via a Monte Carlo approach. Experimentally, measurements of vertically emitted intensity are taken for GaAs PCW membranes with varying amounts of extrinsic disorder. Since the intensity measurements are a direct measure of disordered-induced broadening and frequency shift (blueshift) of the DOS, we compare our computed DOS with the intensity measurements and the two are found to be in very good qualitative agreement. The comparison between our theory and experimental data demonstrates the importance of including local-field effects when computing disorder-induced changes to the eigenfrequencies and eigenmodes of PCWs. While our theory is perturbative, the semianalytical approach is computationally efficient and accurate even for reasonably high amounts of extrinsic disorder and the results offer useful insights in designing disordered PCWs, e.g., for spontaneous emission enhancements of embedded quantum dots. Finally, we also show an example of the underlying disorder-induced quasimodes that can be obtained on a finite-size PC lattice by computing the numerically exact Green function using a full three-dimensional (3D) finite-difference time domain (FDTD) approach [6].

Our paper is organized as follows. In Sec. II we review our formalism for modeling disorder-induced resonance shifts and point out the limitations of some of the polarization models commonly used in the literature for modeling disorder in PCWs. We then introduce our extended polarization model for modeling both intrinsic and extrinsic disorder and show how it results in a nonvanishing first-order frequency shift. In Sec. III, we highlight our approach for computing the disordered DOS given the mean and standard deviation of disorder-induced resonance shifts. We also present a mathematical argument based on photonic Green functions that link the disordered DOS to vertically emitted intensity measurements. In Sec. IV, we numerically compute disorder-induced resonance shifts and the disordered DOS which we compare with experimental

measurements performed on GaAs PCW membranes. While we find qualitatively good agreement with the measurements, in Sec. V we discuss some limitations of the perturbative model and we also show some numerically exact simulations of finite-size PCWs, which are limited in spatial size because of the numerical complexities. In Sec. VI, we summarize the strengths and weaknesses of our perturbative semianalytic approach and discuss our results in the context of previous reports in the literature. We conclude in Sec. VII.

## II. DISORDER-INDUCED RESONANCE SHIFTS AND DISORDER POLARIZATION MODELS

For modeling the effects of disorder on light scattering in PCWs, we focus our attention on deriving the first-order perturbative change to the eigenfrequencies of a dielectric structure. We treat disorder as a perturbation and employ perturbation theory techniques adapted to dielectric structures with high index contrasts [32,34]. We denote the perturbed eigenfrequencies as  $\omega(k) = \omega_0(k) + \Delta\omega(k)$ , where  $\omega_0$  is the unperturbed eigenfrequency,  $k$  represents the wave vector, and  $\Delta\omega$  represents the first-order perturbation. Since disorder in PCWs is statistical in nature, we compute the ensemble average over nominally identical disordered PCWs. Thus the first-order ensemble averaged correction (frequency shift) is given by [29] ( $\omega$  dependence is implicit assuming  $\omega(k)$  is invertible)

$$\mathbb{E}[\Delta\omega] = -\frac{\omega_0}{2} \int_{\text{cell}} \mathbb{E}[\mathbf{E}^*(\mathbf{r}) \cdot \mathbf{P}(\mathbf{r})] d\mathbf{r}, \quad (1)$$

where  $\mathbf{E}(\mathbf{r})$  is the unperturbed eigenmode,  $\mathbf{P}(\mathbf{r})$  is the polarization function to characterize the dielectric disorder, and the integration is carried out over the primitive unit cell of the PC lattice. The fields are normalized according to  $\int_{\text{cell}} \varepsilon(\mathbf{r}) \mathbf{E}^*(\mathbf{r}) \cdot \mathbf{E}(\mathbf{r}) d\mathbf{r} = 1$ , where  $\varepsilon(\mathbf{r})$  is the unperturbed dielectric constant. The rms frequency shift defined by  $\sqrt{\mathbb{E}[\Delta\omega^2]}$ , is computed similarly as [30]

$$\mathbb{E}[\Delta\omega^2] = \frac{\omega_0^2}{4} \iint \mathbb{E}[\mathbf{E}^*(\mathbf{r}) \cdot \mathbf{P}(\mathbf{r}) \mathbf{E}^*(\mathbf{r}') \cdot \mathbf{P}(\mathbf{r}')] d\mathbf{r} d\mathbf{r}'. \quad (2)$$

Statistically,  $\Delta\omega$  is a random variable with  $\mathbb{E}[\Delta\omega]$  as its mean while the variance denoted by  $\sigma^2$  is given as  $\sigma^2 = \mathbb{E}[\Delta\omega^2] - (\mathbb{E}[\Delta\omega])^2$ . Note that Eq. (2) denotes the variance if and only if the mean frequency shift is zero. Hence, given the unperturbed eigenmodes, one is left with choosing a suitable polarization model to describe the perturbation of the PC lattice. Structural disorder in PCWs can be viewed as introducing additional scattering sites in an otherwise perfect PCW lattice. The scattering sites induce extrinsic dipole moments resulting in a disorder-induced polarization which acts as a source term in the homogeneous Maxwell equations, thus contributing to scattering of a propagating Bloch mode. An alternative picture is that the perturbations will disorder the PC band structure and thus the DOS, which will cause disorder-induced localization modes and scattering in directions that might otherwise be forbidden (e.g., a lossless propagating mode will couple to radiation modes above the light line in the case of a PCW slab).

There are typically two models that have been widely used in the photonics community for modeling dielectric perturbations, which we denote as *weak-index contrast*  $\mathbf{P}_w(\mathbf{r})$

and *smooth-perturbation*  $\mathbf{P}_s(\mathbf{r})$ . The former model neglects the problem of field discontinuities at high-index-contrast surfaces, and is well defined for field components that are parallel to the interface; in contrast, the latter model addresses this field-discontinuity problem, though it is appropriate for perturbing a surface uniformly in a perpendicular direction, e.g., displacing a long sidewall in a direction that is perpendicular to the wall interface. By way of a simple example, consider a simple planar interface between two dielectrics (e.g., air and semiconductor slab)  $\varepsilon_a, \varepsilon_s$  where  $\varepsilon_a < \varepsilon_s$ , located at  $\mathbf{r}'$ . When perturbed by a small amplitude  $\Delta h$ , the two polarization models are given as

$$\mathbf{P}_w(\mathbf{r}) = \Delta\varepsilon\Delta h(\mathbf{r})\mathbf{E}(\mathbf{r})\delta(\mathbf{r} - \mathbf{r}'), \quad (3)$$

$$\mathbf{P}_s(\mathbf{r}) = \Delta\varepsilon\Delta h(\mathbf{r})\left(\mathbf{E}_{\parallel}(\mathbf{r}) + \frac{\varepsilon(\mathbf{r})}{\varepsilon_a\varepsilon_s}\mathbf{D}_{\perp}(\mathbf{r})\right)\delta(\mathbf{r} - \mathbf{r}'), \quad (4)$$

where  $\Delta\varepsilon = \varepsilon_a - \varepsilon_s$  and  $\Delta h$  changes sign depending on the direction of the perturbation, i.e., from  $\varepsilon_a$  to  $\varepsilon_s$  or vice versa, and  $\mathbf{E}_{\parallel}(\mathbf{r})$ ,  $\mathbf{D}_{\perp}(\mathbf{r})$  denote the parallel and perpendicular components of the electromagnetic fields relative to the boundary interface. The weak-index contrast model is accurate in systems exhibiting weak-index contrast (i.e.,  $|\Delta\varepsilon| \ll 1$ ) and is the most popular choice for modeling imperfections in dielectric structures such as optical waveguides [35]. In high-index contrast systems such as PCWs, the quantity  $\Delta\varepsilon|\mathbf{E}|^2$  is, however, generally ill-defined at the interface due to a large step discontinuity in  $\mathbf{E}_{\perp}$  [34], hence the smooth-perturbation model is likely more appropriate at the interface due to the use of continuous field components. The smooth-perturbation model is expected to be valid as long as the perturbation is smooth. Both models have been used to compute disorder-induced losses in PCWs [14,16,30,36] and have yielded a good qualitative understanding of the observed disorder-induced loss phenomena.

If one views the perturbation (smooth or piecewise smooth) as introducing scatterers into the system, one must take into account their respective polarizabilities which in general depend on the direction of the perturbation. The weak-index contrast and smooth-perturbation models assign polarizabilities that differ only in sign when the direction of perturbation is reversed but remain unchanged in magnitude. Moreover, the magnitude of the polarizability of a scatterer can be drastically different in the weak-index approximation as demonstrated by the example of a small dielectric sphere in a homogeneous background (see Ref. [37]). Therefore, in general for piecewise smooth perturbations such as bumps on an interface, it is important to compute polarizabilities that correctly take into account the direction of perturbation. To address this concern, Johnson *et al.* [32] introduced the *bump-perturbation* polarization model, denoted by  $\mathbf{P}_b(\mathbf{r})$  to model surface roughness in PCWs as piecewise smooth bumps on the interface, where

$$\mathbf{P}_b(\mathbf{r}) = [\varepsilon_{\text{avg}}\alpha_{\parallel}\mathbf{E}_{\parallel}(\mathbf{r}) + \varepsilon(\mathbf{r})\gamma_{\perp}\mathbf{D}_{\perp}(\mathbf{r})]\Delta V\delta(\mathbf{r} - \mathbf{r}'), \quad (5)$$

where  $\varepsilon_{\text{avg}} = (\frac{\varepsilon_a + \varepsilon_s}{2})$ , and  $\alpha_{\parallel}$ ,  $\gamma_{\perp}$  denote the polarizabilities (polarizability tensors per unit volume) of the bump perturbation and  $\Delta V$  is the volume of the disorder bump element. This model is valid for arbitrary dielectric contrasts and bump shapes, and useful formulas have been obtained for rectangular

and cylindrical shaped bumps [32]. Using the polarizabilities for a cylindrical bump shape, this polarization model has been used to model resonance shifts caused by intrinsic disorder in PCWs [30] where a mean blueshift and broadening of the ideal band structure was found. As was noted in Ref. [30], resonance shifts in the band structure are not predicted by either the weak-index contrast or the smooth-perturbation models.

In this work, we apply the bump-perturbation model with cylindrical bump shape polarizabilities, to compute disorder-induced resonance shifts in PCWs, and systematically investigate what happens with an increase in the disorder parameters for shifted holes. We use this model to connect to related experiments on deliberately disordered GaAs membranes where embedded quantum dots couple to disorder-induced localized modes resulting in enhanced spontaneous emission [26,33]. The PCW we consider is a standard W1 formed by introducing a line defect in a triangular lattice of air holes etched in a semiconductor slab, Fig. 1(a). The air holes are cylinders so we employ cylindrical coordinates  $(r, \theta, z)$  henceforth. Furthermore, the disordered air hole is assumed to have a constant cross section throughout the slab thickness. This allows us to replace the disorder volume element in Eq. (5) by its cross-sectional area  $\Delta A$  and the polarizabilities are now  $2 \times 2$  tensors representing polarizability per unit area [32] and approximating to first order, the perturbed area  $\Delta A$  of the disorder element is proportional to  $|\Delta h|$ .

In light of current experiments studying localization modes and resonance shifts as a function of deliberate disorder, we extend the disorder model of Ref. [30] to deal with both intrinsic and varying extrinsic disorder (e.g., through a systematic increase of the external disorder parameters). While the previous model considered rapid radial fluctuations of the air-slab interface as the source of intrinsic disorder, here we model both intrinsic and extrinsic disorder as a net center shift of the air hole as shown schematically in Fig. 1(b). Although intrinsic disorder is likely best described by rapid radial fluctuations, the choice to model intrinsic disorder as

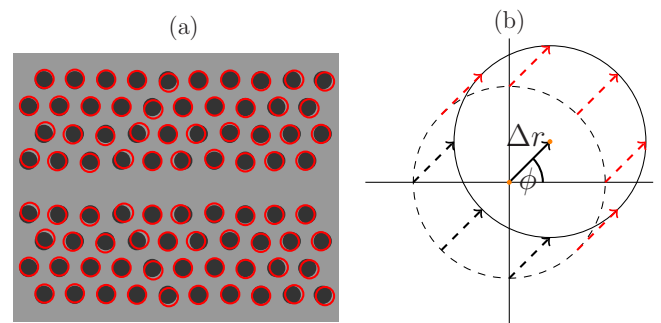


FIG. 1. (Color online) (a) Schematic of a disordered W1 with ideal air holes (solid dark (black) circles), disordered holes (light (red) circles), and the background slab (gray). (b) Schematic of a hole center shift with the centers marked by solid light (orange) circles and the direction of perturbation given by the solid-black arrow. The magnitude of the perturbation is denoted by  $\Delta r$  and the azimuthal direction or angle of the perturbation is given by  $\phi$ . Dashed arrows indicate the shifts of the air-slab interface with dashed-light (red) and dashed-dark (black) arrows representing positive and negative shifts, respectively.

a hole center shift is driven by simplicity as one can map rapid radial fluctuations to an effective hole center shift by comparing experimental loss data with numerical simulations as demonstrated by Garcia *et al.* [38]; also, the main effect of the disorder below is certainly through deliberate disorder.

Since disorder is stochastic in nature, we denote  $(\Delta h, \phi)$  as the random variables quantifying the total disorder (extrinsic and intrinsic) in PCWs. The net magnitude of the shift  $|\Delta h|$  is constant around the circumference while the sign is determined by the net azimuthal direction of the shift, denoted by  $\phi$  [see Fig. 1(b)]. The shift of an infinitesimally small arc lying on the circular air-slab interface is then given by

$$\Delta h(\Delta r, \phi; \theta) = \begin{cases} +\Delta r, & \phi \in \Omega, \\ -\Delta r, & \phi \notin \Omega, \end{cases} \quad (6)$$

where  $\Omega = [\theta - \frac{\pi}{2}, \theta + \frac{\pi}{2}]$ ,  $\theta$  denotes the polar coordinate and  $\Delta r$  quantifies the magnitude of the net radial perturbation. A positive bump or shift ( $+\Delta r$ ) is defined as the air-slab boundary shifting into the slab and vice versa for negative bumps or shifts as illustrated in Fig. 1(b). We denote  $\Delta r_{i/e} \sim |\mathcal{N}(0, \sigma_{i/e})|$ ,  $\phi_{i/e} \sim \mathcal{U}[-\pi, \pi]$  as the random variables for the radial magnitudes and azimuthal directions of the intrinsic and extrinsic disorder perturbations, respectively;  $\mathcal{N}(\mu, \sigma)$  denotes a normal distribution with mean  $\mu$  and standard deviation  $\sigma$  while  $\mathcal{U}[a, b]$  denotes a uniform distribution over the interval  $[a, b]$ . The net radial fluctuation can be broken down into its Cartesian components  $\Delta x$ ,  $\Delta y$ , which are given below:

$$\Delta x = \Delta r_i \cos(\phi_i) + \Delta r_e \cos(\phi_e), \quad (7)$$

$$\Delta y = \Delta r_i \sin(\phi_i) + \Delta r_e \sin(\phi_e). \quad (8)$$

The net radial fluctuation is then given as  $\Delta r = \sqrt{\Delta x^2 + \Delta y^2}$  while the net azimuthal direction is simply  $\phi = \tan^{-1}(\frac{\Delta y}{\Delta x})$ . Comparing to our previous model of rapid radial fluctuations [30], this model lacks the concept of an intrahole correlation length as all points on the hole shift by the same magnitude but in different directions depending on the angular hole coordinate  $\theta$ . However this model is more appropriate for modeling the deliberate displacement of the disordered holes performed in the experiment.

To highlight the main difference between the three polarization models discussed earlier, let's compute the ensemble averaged first-order frequency shift  $\mathbb{E}[\Delta\omega]$  by using Eqs. (3), (4), or (5) in Eq. (1). For weak-index contrast and smooth-perturbation models, one must compute the expectation of the total disorder  $\mathbb{E}[\Delta h]$ . If the extrinsic disorder is zero ( $\sigma_e = 0$ ), it is trivial to show that  $\mathbb{E}[\Delta h] = 0 \rightarrow \mathbb{E}[\Delta\omega] = 0$ . In the case where both intrinsic and extrinsic disorder are present, one can still show  $\mathbb{E}[\Delta h] = 0$  as can be verified via a Monte Carlo simulation. This result is expected because given any random value for the net radial displacement  $\Delta r$ , all possible azimuthal directions are equally likely; and since we are assigning symmetric weights (differing only in sign) to positive and negative shifts in these two models, the first-order correction vanishes. This is in line with previous findings where intrinsic disorder was modeled as rapid radial fluctuations [30]. However, a nonzero first-order mean frequency shift is expected to occur for the bump-perturbation model since  $\mathbb{E}[\alpha_{\parallel}|\Delta h] \neq 0$ ,  $\mathbb{E}[\gamma_{\perp}|\Delta h] \neq 0$ . This is because the polarizabilities for the shifts that we use in Eq. (5)

are *asymmetric*, i.e.,  $\alpha_{\parallel}^+ \neq \alpha_{\parallel}^-$ ,  $\gamma_{\perp}^+ \neq \gamma_{\perp}^-$  where  $+/-$  denote positive and negative shifts respectively.

For  $\mathbb{E}[\Delta\omega^2]$ , none of the expectation terms vanish and therefore the variance  $\sigma^2$  of the first-order frequency shift is positive definite for all three polarizability models as long as  $\mathbb{E}[\Delta\omega^2] \geq \mathbb{E}[\Delta\omega]^2$ . One way to test which model is more appropriate is to compare with experiments where the amount of disorder can be controlled, and that is precisely what we do in Sec. IV.

### III. DISORDERED DENSITY OF STATES AND CONNECTION TO EXPERIMENTS OF VERTICAL LIGHT EMISSION

Since disorder acts to shift and broaden the mode edge, a useful quantity for experimental comparison is the DOS  $\rho(\omega(\mathbf{k}))$ , defined as the number of frequency levels per unit volume of  $\mathbf{k}$  space. Unlike the concept of band structure, which is only well-defined in perfectly periodic systems, the DOS is valid for all structures. It is well known that the DOS of an ideal PCW diverges at the mode edge since the group velocity vanishes, while for a disordered PC structure, the ensemble averaged DOS exhibits a broadened peak around the ideal mode edge where the width of the peak is proportional to the amount of disorder present in the PC structure [39].

To compute the DOS, we first remark that the definition of DOS bears close resemblance to the mathematical definition of a probability density function (PDF). Hence, just like a histogram generated from a large sample dataset represents the underlying PDF, the histogram generated from a band structure represents the DOS. To compute a disordered DOS instance, we generate a histogram denoted by  $\rho_i(\omega)$  from the disordered band structure given by  $\omega_i(k) = \omega_0(k) + \Delta\omega_i(k)$  where  $\Delta\omega_i$  is sampled from an underlying probability distribution. One then computes the ensemble averaged disordered DOS by averaging over  $N$  disordered DOS instances  $\bar{\rho}(\omega) = \sum_i \rho_i(\omega)/N$ .

The key quantity here is the underlying probability distribution of the random variable  $\Delta\omega$ . If one discretizes the integral in Eq. (1), one sees that  $\Delta\omega$  is a sum over a large number of random variables that are neither identically distributed or independent in general. But since the underlying random variables ( $\Delta r_{i/e}, \phi_{i/e}$ ) characterizing the disorder in our PCW samples have well defined bounded moments of all order, we can invoke the central limit theorem from probability theory (especially its extension to dependent stochastic processes) and assume that  $\Delta\omega$  is normally distributed, i.e.,  $\Delta\omega \sim \mathcal{N}(\mathbb{E}[\Delta\omega], \sigma)$ .

Experimentally, the DOS can be obtained by spatially averaging the vertically emitted light intensity measurements in PCWs. To appreciate how the waveguide DOS can be measured through vertical emission, consider the waveguide mode Green function without any disorder [40]:

$$\mathbf{G}_{\text{wg}}(\mathbf{r}, \mathbf{r}'; \omega) = \frac{ia\omega}{2v_g} [\Theta(x - x') \mathbf{f}_k(\mathbf{r}) \mathbf{f}_k^*(\mathbf{r}') e^{ik(x-x')} + \Theta(x - x') \mathbf{f}_k^*(\mathbf{r}') \mathbf{f}_k(\mathbf{r}) e^{-ik(x-x')}], \quad (9)$$

where  $a$  is the pitch,  $v_g$  is the group velocity,  $\Theta(x - x')$  is the Heaviside function, and  $\mathbf{f}_k$  is the ideal Bloch mode for modes below the light line. Now consider adding a point

disorder model, where the disorder causes a polarizability with a Lorentzian line shape (e.g., typical of a disorder-induced resonance or an embedded light source such as a quantum dot),  $\alpha^d = A/(\omega_0 - \omega - i\gamma)$ , where  $\omega_0$  is the disorder induced resonance frequency,  $\gamma$  is the broadening of the resonance, and  $A$  is the coupling strength. Using a Dyson equation,  $\tilde{\mathbf{G}} = \mathbf{G} + \mathbf{G}\alpha^d\tilde{\mathbf{G}}$ , the Green function in the presence of the perturbation can be exactly obtained through  $\tilde{\mathbf{G}}$ , where  $\alpha^d$  has units of volume (polarizability volume) and the Green function has units of inverse volume. Defining  $\rho_i(\mathbf{r}_d) \equiv \text{Im}[\mathbf{G}_{ii}(\mathbf{r}_d, \mathbf{r}_d)]$  where  $\text{Im}[\ ]$  denotes the imaginary component as a measure of the (projected) LDOS, we obtain

$$\tilde{\rho}_i(\mathbf{r}_d, \omega) = \rho_i(\mathbf{r}_d, \omega) \frac{(\omega - \omega_0)^2 + \gamma[\gamma + A\rho_i(\mathbf{r}_d, \omega)]}{(\omega - \omega_0)^2 + [\gamma + A\rho_i(\mathbf{r}_d, \omega)]^2}, \quad (10)$$

and thus the disordered LDOS now contains signatures of the original waveguide LDOS and the underlying resonance of the disorder site. Looking at the limit  $\omega \rightarrow \omega_0$ ,

$$\tilde{\rho}_i(\mathbf{r}_d, \omega_0) = \rho_i(\mathbf{r}_d, \omega_0) \frac{\gamma}{\gamma + A\rho_i(\mathbf{r}_d, \omega_0)}, \quad (11)$$

where we note that the LDOS at the mode edge is no longer divergent, and instead  $\tilde{\rho}_i(\mathbf{r}_d, \omega_e) = \gamma/A$  (assuming  $\omega_0 = \omega_e$ ), which is simply the LDOS from the disordered polarizability model. Since this disordered LDOS is now connected to light propagation away from the waveguide through  $\gamma$ , vertically emitted light will clearly contain signatures of the disordered LDOS for the waveguide modes, and thus the disordered DOS when spatially integrated.

An alternative picture of the disordered DOS can be obtained by connecting directly to a sum over the disorder-induced modes. In PCWs, due to disorder, propagating and localized modes couple with radiation modes above the light line resulting in vertically emitted intensity. Near the mode edge, the DOS increases due to vanishing group velocity leading to an increase in the radiation loss rate and a broadened peak in the vertically emitted intensity spectrum. Other peaks in the spectrum near the mode edge indicate the presence of disorder-induced localized modes. Given that the vertically emitted intensity is proportional to the radiation loss rate, denoted by  $\gamma$ , one can show that the radiation loss rate is proportional to the DOS. Let us assume the disordered quasimodes (or ‘‘quasinormal modes’’) [41] are known or can be computed, denoted by  $\tilde{\mathbf{f}}_j(\mathbf{r})$  where  $j$  indexes the quasimodes which have complex eigenfrequencies  $\tilde{\omega}_j = \omega_j + i\gamma_j$ , where the quality factor of each resonance is  $Q_j = \omega_j/2\gamma_j$ . Then using mode expansion, one obtains the Green function of the disordered PCW by an expansion over the quasinormal modes [42,43],

$$\mathbf{G}_{\text{dis}}(\mathbf{r}, \mathbf{r}'; \omega) = \sum_j \frac{\omega^2}{2\tilde{\omega}_j(\tilde{\omega}_j - \omega)} \tilde{\mathbf{f}}_j(\mathbf{r})\tilde{\mathbf{f}}_j(\mathbf{r}'), \quad (12)$$

and the LDOS of the disordered PCW is

$$\rho(\mathbf{r}, \omega) = \frac{2}{\pi\omega} \text{Im}[\text{Tr}[\mathbf{G}_{\text{dis}}(\mathbf{r}, \mathbf{r}; \omega)]], \quad (13)$$

where  $\text{Tr}[\ ]$  denotes the trace. From the total LDOS one can compute the DOS by integrating over all space. Therefore one sees that the radiation loss rate and the vertically emitted intensity are inherently linked to the disordered DOS. Indeed,

each one of the underlying quasimodes (and every disordered element) has a vertical decay channel associated with vertical decay above the light line.

#### IV. CALCULATIONS AND MEASUREMENTS OF THE DISORDERED-INDUCED RESONANCE SHIFTS AND DENSITY OF STATES

The experimental samples are W1 GaAs membranes with a pitch of  $a = 240$  nm and thickness 150 nm with an embedded layer of InAs self-assembled quantum dots at the center of the membrane having uniform density of  $80 \mu\text{m}^{-2}$ . Quantum dots present a very similar refractive index to that of the surrounding membrane material (GaAs) and are included in the sample to facilitate easier excitation of a broad range of photonic modes of the disordered system, which has been used elsewhere to study the modified emission of quantum dots coupled to disorder-induced resonances [26]. However, the experiments presented in this paper are carried out under high excitation power ( $57 \mu\text{W}/\text{m}^2$ ) [33], which drives the quantum dots beyond saturation, and they become transparent. Consequently, we consider negligible quantum dot contribution to both inelastic and elastic scattering and, thus, we can rule out any quantum dot contribution to our model.

Various samples each measuring  $100 \mu\text{m}$  long are manufactured with varying degrees of extrinsic disorder. Extrinsic disorder is introduced via an additional hole center displacement characterized by  $\sigma_e$  and is varied from  $0.01a = 2.4$  nm to  $0.05a = 12$  nm in  $0.01a = 2.4$  nm steps. The samples are excited and vertically emitted intensity is collected as function of wavelength and position along the waveguide direction  $I(\lambda, x)$  as shown in Figs. 3(a) and 3(b). The intensity is then spatially integrated along the waveguide  $I(\lambda) = \int I dx$  as shown in Fig. 3(c).

To connect to these experiments, we model a corresponding W1 PCW [see Fig. 1(a)] with a slab dielectric constant suitable for GaAs ( $\epsilon = 12.11$ ), with the following parameters:  $r = 0.295a$  (hole radius),  $h = 0.625a$  (slab height). The ideal band structure (i.e., with no disorder) is plotted in Fig. 2(a), depicting the fundamental lossless guided mode that spans from 876 nm (thereafter going above the light line) to 930 nm (mode edge). The intrinsic disorder, kept fixed at  $\sigma_i = 0.005a = 1.2$  nm is characterized by an effective hole-center shift and determined from comparing the experimental far-field intensity spectra of PCWs with varying amounts of extrinsic disorder to numerical FDTD simulations of the spectra. More specifically, one compares the width of the Lifshitz tail present in both spectra which depends on the amount of disorder in the structure (see Ref. [38] for details).

The mean and standard deviation of  $\Delta\omega$  in units of free-space wavelength, assuming the bump-perturbation model for all samples, are plotted in Figs. 2(b) and 2(d). For the conversion of units, since  $\omega \gg \Delta\omega$  we use the formulas  $\mathbb{E}[\Delta\lambda] = -2\pi c \mathbb{E}[\Delta\omega]/\omega^2$ ,  $\mathbb{E}[\Delta\lambda^2] = 4\pi^2 c^2 \mathbb{E}[\Delta\omega^2]/\omega^4$  where  $c$  is the speed of light in vacuum. The expectations in Eqs. (1) and (2) were computed numerically, that is given the statistical parameters for disorder,  $10^4$  samples of the set  $(\Delta r_i, \Delta r_e, \phi_i, \phi_e)$  are drawn from the underlying probability distributions which yields  $10^4$  samples of  $\Delta h$ . The integration is carried out via Riemann sums where the step size is chosen

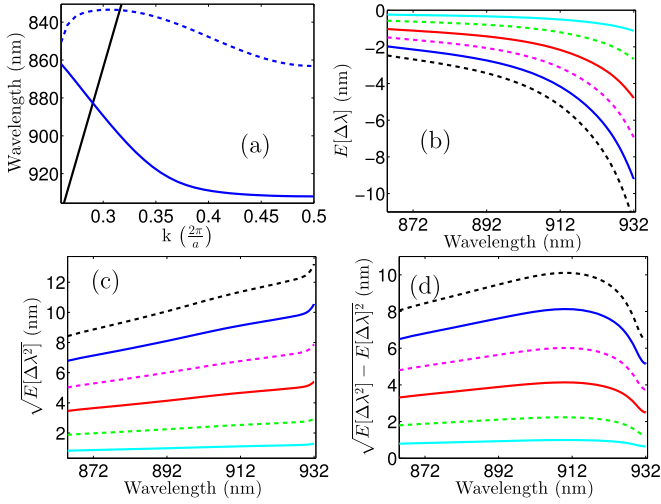


FIG. 2. (Color online) (a) Photonic band structure (in units of wave vector vs vacuum wavelength) of the ideal  $W1$  showing the fundamental (solid) and higher order (dashed) guided modes. The light line is shown in black. (b) Mean frequency shift  $\mathbb{E}[\Delta\omega]$  for six disordered samples for the fundamental guided mode. (c) RMS frequency shift  $\sqrt{\mathbb{E}[\Delta\omega^2]}$  representing the standard deviation if and only if the mean frequency shift is zero. (d) Standard deviation of  $\Delta\omega$  given a nonzero mean frequency shift (b). In all three graphs, the *intrinsic* disorder is kept fixed at  $0.005a$  (1.2 nm) while the external disorder is varied as follows:  $0a$  [solid light gray (cyan)],  $0.01a$  (2.4 nm) [dashed light gray (green)],  $0.02a$  (4.8 nm) [solid medium gray (red)],  $0.03a$  (7.2 nm) [dashed medium gray (magenta)],  $0.04a$  (9.6 nm) [solid dark gray (blue)],  $0.05a$  (12 nm) (dashed black).

to be small enough (3 nm in our case) to ensure numerical convergence.

From Fig. 2(b), we see that for all cases of disorder, the mean frequency shift is a *blueshift* that increases as one approaches the mode edge and as the total amount of disorder increases. We note that the prediction of a mean blueshift is nontrivial and is solely due to the asymmetric polarizabilities present in the bump-perturbation polarization model. Regardless of the polarization model employed, the rms frequency shift is nonzero as shown in Fig. 2(c) which is equivalent to the standard deviation if and only if the weak-index contrast or smooth-perturbation polarization models are employed [39]. Figure 2(c) implies that in the absence of a mean shift, the band structure or DOS broadens monotonically as one approaches the mode edge for any given amount of extrinsic disorder. In the presence of a nonzero mean shift (blueshift), the standard deviation is modified as shown in Fig. 2(d) which shows that broadening is nonmonotonic. In fact, for any given amount of extrinsic disorder, as one approaches the waveguide mode edge, the magnitude of the blueshift increases but the broadening actually decreases. Since one is most often concerned with the mode edge or cutoff of the fundamental guided mode in PCWs, we find that the mode-edge mean blueshift is roughly of the same order as the amount of total disorder (i.e., extrinsic + intrinsic) in the system, while the standard deviation of the blueshift is roughly half the amount of total disorder. For example, for extrinsic disorder  $\sigma_e$  of

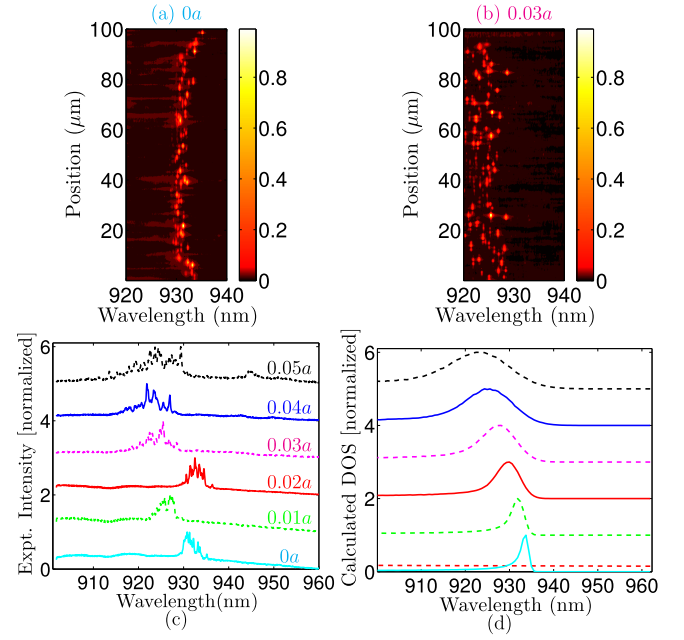


FIG. 3. (Color online) (a) and (b) Experimental normalized intensity spectra obtained by scanning along the waveguide position for two different amounts of extrinsic disorder as indicated in the figure. (c) Experimental spatially integrated intensity for varying degrees of extrinsic disorder as labeled in the figure. (d) Calculated ensemble averaged DOS (normalized) for the fundamental waveguide mode for the six disordered samples in (c). The red-dashed line in the lowest disorder case is given by  $A \frac{\lambda_{\text{min}}^2}{\lambda^2}$  with  $A = 0.2$  and represents the qualitative contribution of radiation modes to the DOS. The amount of intrinsic disorder in all samples is  $\sigma_i = 0.005a$  (1.2 nm).

$0.02a$  (4.8 nm), then the mode edge is blueshifted roughly by 4.8 nm with a standard deviation of approximately 2.5 nm.

The normalized experimental intensity spectra for two different amounts of extrinsic disorder along the waveguide is shown in Figs. 3(a) and 3(b). Integrating along the waveguide direction, the corresponding intensity spectra is compared to the ensemble averaged disordered DOS for the six samples (considered previously in Fig. 2) in Figs. 3(c) and 3(d). For now we neglect the contribution of radiation modes to the DOS which scales roughly as  $1/\lambda^2$  [please see Fig. 3(d) for what this might look like]. Treating the DOS as a probability distribution as mentioned in Sec. III, each DOS instance histogram has a sample size of 1000 (number of  $k$  points) and bin resolution of 0.27 nm (200 bins). The ensemble-averaged disordered DOS was calculated from 500 disordered DOS instances. Note that, as discussed earlier, the DOS at the mode edge formally diverges (as the group velocity approaches zero) in the absence of disorder but our computed disordered DOS is nondivergent and shows a pronounced mean blueshift as well as broadening caused by the variance of the frequency shift. This agrees qualitatively well with the experimental intensity spectra except for the case of  $\sigma_e = 0.02a$  (4.8 nm); where the theory predicts a blueshift, but the experimental intensity spectrum is redshifted. The observed redshift of the mode-edge is within the computed standard deviation so it is either that this discrepancy arises due to the experimental sample representing only one disorder instance or the fabrication method of these

particular waveguides where, e.g., a proximity effect could introduce an additional unknown degree of disorder different from the designed one.

Strictly speaking, our perturbation theory computes mode-edge resonance shifts and broadening for *periodically* disordered PCWs; that is the primitive unit cell is disordered and then repeated indefinitely. This is an approximation as in reality the disordered PCW is a concatenation of disordered unit cell instances sampled from an underlying probability distribution. Moreover in the experimental intensity spectra [Fig. 3(c)], we can see the signature of localized modes forming around the mode edge for all cases of disorder which our computed DOS cannot reproduce since localized modes that form due to cavity-like defects are naturally not present in a waveguide exhibiting periodic disorder. Hence the shift and broadening of the DOS caused by localized modes particularly above the mode edge is absent from our calculation.

To assess the role of multiple scattering qualitatively, we considered incoherent disorder-induced losses in our samples, with and without multiple scattering. With the mode edge roughly corresponding to a group index of  $n_g \approx 50$ , our computations indicate that for  $n_g > 20$ , we are already in the regime of multiple scattering for all amounts of disorder. Therefore, akin to the absence of sharp features in the transmission spectrum without multiple scattering [44], the *periodic* disorder perturbative approach lacks the sharp features shown in the experimental intensity spectra especially above the mode edge so for more realistic predictions, a nonperturbative approach would be needed that takes into account multiple-scattering effects. Such an approach is numerically very demanding and is beyond the scope of this first paper on the topic. However, below we show some numerically exact solutions of disorder-induced resonances and LDOS for short length PCWs.

## V. NUMERICALLY COMPUTED DISORDERED LDOS INSTANCES FROM A FINITE-SIZE PCW

Having identified the possible limits of perturbation theory above, we now present some brute force calculations of the LDOS using full 3D FDTD computations in a disordered PCW lattice. The numerical complexity is very demanding so we are restricted to much smaller waveguide lengths than used in the experiment; also, we can only compute a small number of instances which are not enough to compute the ensemble average trend shown in Fig. 3. This is mainly due to the large memory requirements of the simulation volume since it cannot be reduced by using symmetric boundary conditions due to symmetry breaking caused by disorder. Nevertheless, such calculations are useful for getting a physical picture of what is happening for a particular instance and section of a disordered PCW.

To show that the DOS varies from instance to instance given the disorder is kept fixed, we calculate the projected LDOS  $\rho_\mu(\mathbf{r}, \omega)$  for ten statistically disordered finite-length PCWs, as shown in Fig. 4, by directly computing the numerically exact photonic Green function of the PCW (see Ref. [6] for numerical implementation details) using the 3D FDTD method [45]. The samples we simulate are  $7.2 \mu\text{m}$  long (30 unit cells). With the waveguide cross section in the  $xy$  plane,

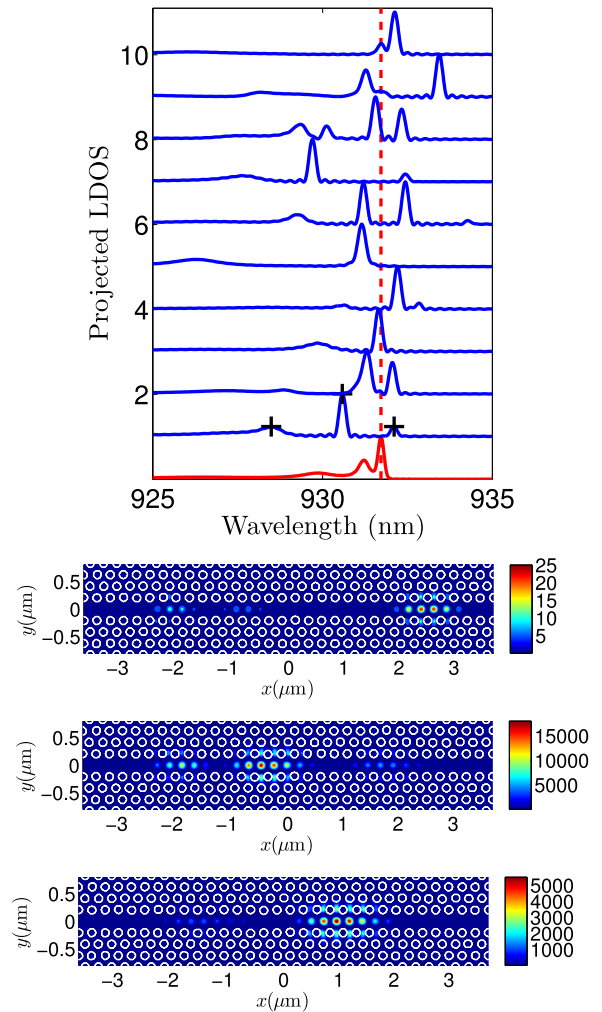


FIG. 4. (Color online) Top: Projected LDOS values of a  $y$ -oriented dipole centered at the antinode of  $\mathbf{E}_y$ , computed for ten instances of disorder [dark solid (blue)] with internal and external disorder values of  $\sigma_i = 0.005a$  (1.2 nm),  $\sigma_e = 0.02a$  (4.8 nm) respectively. For reference, the LDOS with no *extrinsic* disorder [light solid (red)] and ideal mode-edge [dashed light (red) vertical line] are also shown. All LDOS instances are normalized to their own LDOS peak. The length of the waveguides was kept fixed at  $7.2 \mu\text{m}$  (30 unit cells). Bottom: As highlighted by the black markers (+) on the Projected LDOS instance, starting from above (right) and going below (left) the ideal mode edge, disorder-induced localized mode intensity  $|\mathbf{E}_y|^2$  is shown.

denoting the waveguide direction as  $x$  and the origin at the center of the waveguide, we compute the LDOS of a  $y$ -oriented dipole  $\rho_y(0, \omega)$  placed at the antinode of the disorder-induced mode component  $\mathbf{E}_y$ , which occurs at the origin. The intrinsic and extrinsic disorder values are  $0.005a$  (1.2 nm),  $0.02a$  (4.8 nm), respectively. While ten instances which are only 30 unit cells long are not enough to conclude the existence of a mean blueshift of the mode edge, the deviations of the mode edge in the LDOS profiles are within the calculated standard deviation shown in Fig. 2(d). This may partially explain the discrepancy observed in Fig. 3(c) for  $\sigma_e = 0.02a$  (4.8 nm) as the experimental sample represents one disordered instance. For completeness, Fig. 4 also shows examples of disorder-

induced localized modes that appear both above and below the mode edge. These modes are formed via multiple scattering in cavity-like defects introduced via disorder.

We highlight that we have found that a 2D FDTD method, despite being at least one order of magnitude quicker and allowing us to simulate very long sample lengths, to be inadequate for computing a realistic Green function and LDOS for the 3D PCW slab. First, the mode edge for a 2D PCW with the same structural parameters (apart from the slab height) is different ( $1.2 \mu\text{m}$ ) and second, a 2D PCW does not possess radiation or leaky modes and out-of-plane decay cannot be computed. Hence the computed 2D Green functions and LDOS are different from its 3D counterparts and do not accurately capture the realistic 3D resonance shifts. Although a 2D calculation can capture the qualitative modal profile of the localized modes, their sensitivity to disorder is quite different to 3D quasimodes. Thus in general one requires a 3D FDTD model to compute the LDOS for a PCW slab.

## VI. DISCUSSION AND CONNECTIONS TO PREVIOUS WORKS

Our theory, though perturbative, provides an intuitive and computationally efficient semianalytical approach to producing experimentally relevant results for high amounts of extrinsic disorder. One ensemble average DOS computation which includes computing the ideal Bloch modes, Monte Carlo runs for the expectations, and Riemann integrals for a given amount of disorder takes roughly 3 h on a single-core CPU whereas computing the LDOS of a  $7.2 \mu\text{m}$  long disordered PCW using 3D FDTD takes approximately 10 CPU h for *each* disorder instance on a cluster using 20 multicore CPU nodes.

As we have stated before, the bump-perturbation polarization model is crucial to our findings. It is not the exact shape of the bump that is important (see Refs. [29,32]) but the use of asymmetric polarizabilities that yields a nonzero mean frequency shift. In the context of disorder-induced losses where all three polarization models produce similar results, previously we have argued that the bump polarization model should be best suited for modeling disorder characterized via rapid radial fluctuations and the smooth-perturbation model should be valid as long as the air-slab interface remains nearly circular [30] which is indeed the case considered in this work. To resolve this ambiguity, we rely on the comparison with experimental findings (see Sec. IV) which indicates that the bump-polarization model (in the absence of any other models proposed in the literature) is likely best suited for all types of disorder and various disorder-induced phenomena in PCWs.

Reference [30] highlighted the importance of accounting for local-field effects in PCWs by computing disorder-induced resonance shifts for the three polarization models mentioned in Sec. II. While the impact of disorder on the DOS is

qualitatively well known, to our knowledge, no one has quantified the expected resonance shifts or spectral broadening as a function of disorder and computed the disordered DOS which is found to be in good qualitative agreement with experiments. Previously, spectral broadening of the band structure was observed experimentally by Le Thomas *et al.* [46] and predicted theoretically by Savona [31] whose findings showed increased spectral broadening of the band structure as the disorder increases, but did not predict a blueshift or quantify the expected shift or broadening as a function of disorder. In the absence of a blueshift, Fussell *et al.* also showed theoretical broadening of the DOS in coupled-PC-cavity waveguides [39]. While it is generally accepted in the community that broadening increases monotonically as one approaches the mode edge, our findings show that in the presence of a mean blueshift, the broadening actually decreases as one approaches the mode-edge. This implies that the blueshift effect is more dominant than broadening at the mode edge and should be taken into account.

## VII. CONCLUSIONS

Through theory and experiment, we have shown that accurate modeling of local-field effects is critical for computing experimentally relevant mean frequency shifts and realistic DOS profiles in PCWs. These findings also point out the possible limitations of disorder polarization models that do not include local-field effects or include local-field effects through the use of symmetric polarizabilities. For extrinsic disorder values up to 12 nm, our computationally efficient perturbative approach yields results that are in very good qualitative agreement with experiments and can be used to compute realistic quantities such as Purcell factor enhancements in PCWs with embedded quantum dots. We have also shown examples of the numerically exact LDOS for various disordered instances and the underlying disorder-induced resonance modes on a small PCW using a rigorous 3D FDTD approach. Future work could focus on developing a nonperturbative approach that takes into account multiple scattering to better model the localized modes that appear above the mode edge.

## ACKNOWLEDGMENTS

This work was supported by the Natural Sciences and Engineering Research Council of Canada (NSERC) and Queen's University, Canada. A.J., P.D.G., and P.L. gratefully acknowledge the financial support from the Danish Council For Independent Research (Natural Sciences and Technology and Production Sciences), the Villum Foundation, and the European Research Council (ERC Consolidator Grant No. "ALLQUANTUM").

- 
- [1] T. F. Krauss, *Nat. Photon.* **2**, 448 (2008).  
 [2] P. Lodahl, S. Mahmoodian, and S. Stobbe, *Rev. Mod. Phys.* **87**, 347 (2015).  
 [3] T. Yoshie, A. Scherer, J. Hendrickson, G. Khitrova, H. M. Gibbs, G. Rupper, C. Ell, O. B. Shchekin, and D. G. Deppe, *Nature (London)* **432**, 200 (2004).

- [4] K. Hennessy, A. Badolato, M. Winger, D. Gerace, M. Atatüre, S. Gulde, S. Fält, E. L. Hu, and A. Imamoglu, *Nature (London)* **445**, 896 (2007).  
 [5] T. Lund-Hansen, S. Stobbe, B. Julsgaard, H. Thyrrstrup, T. Sünner, M. Kamp, A. Forchel, and P. Lodahl, *Phys. Rev. Lett.* **101**, 113903 (2008).

- [6] P. Yao, V. S. C. Manga Rao, and S. Hughes, *Laser Photon. Rev.* **4**, 499 (2010).
- [7] A. Laucht, S. Pütz, T. Günthner, N. Hauke, R. Saive, S. Frédérick, M. Bichler, M.-C. Amann, A. W. Holleitner, M. Kaniber, and J. J. Finley, *Phys. Rev. X* **2**, 011014 (2012).
- [8] P. Colman, C. Husko, S. Combrié, I. Sagnes, C. W. Wong, and A. De Rossi, *Nat. Photon.* **4**, 862 (2010).
- [9] C. Monat, M. Spurny, C. Grillet, L. O’Faolain, T. F. Krauss, B. J. Eggleton, D. Bulla, S. Madden, and B. Luther-Davies, *Opt. Lett.* **36**, 2818 (2011).
- [10] J. Li, L. O’Faolain, and T. F. Krauss, *Opt. Express* **20**, 17474 (2012).
- [11] N. Skivesen, A. Têtu, M. Kristensen, J. Kjems, L. H. Frandsen, and P. I. Borel, *Opt. Express* **15**, 3169 (2007).
- [12] J. Topol’ančik, P. Bhattacharya, J. Sabarinathan, and P. C. Yu, *Appl. Phys. Lett.* **82**, 1143 (2003).
- [13] T. Baba, *Nat. Photon.* **2**, 465 (2008).
- [14] S. Hughes, L. Ramunno, J. F. Young, and J. E. Sipe, *Phys. Rev. Lett.* **94**, 033903 (2005).
- [15] D. Gerace and L. C. Andreani, *Opt. Lett.* **29**, 1897 (2004).
- [16] B. Wang, S. Mazoyer, J. P. Hugonin, and P. Lalanne, *Phys. Rev. B* **78**, 245108 (2008).
- [17] W. Song, R. A. Integlia, and W. Jiang, *Phys. Rev. B* **82**, 235306 (2010).
- [18] L. O’Faolain, T. P. White, D. O’Brien, X. Yuan, M. D. Settle, and T. F. Krauss, *Opt. Express* **15**, 13129 (2007).
- [19] F. Wang, J. S. Jensen, and O. Sigmund, *Photon. Nanostruct. Fundam. Appl.* **10**, 378 (2012).
- [20] N. Mann, S. Combrié, P. Colman, M. Patterson, A. De Rossi, and S. Hughes, *Opt. Lett.* **38**, 4244 (2013).
- [21] L. O’Faolain, S. Schulz, D. M. Beggs, T. P. White, M. Spasenović, L. Kuipers, F. Morichetti, A. Melloni, S. Mazoyer, J. P. Hugonin, P. Lalanne, and T. F. Krauss, *Opt. Express* **18**, 27627 (2010).
- [22] J. Sancho, J. Bourderionnet, J. Lloret, S. Combrié, I. Gasulla, S. Xavier, S. Sales, P. Colman, G. Lehoucq, D. Dolfi, J. Capmany, and A. De Rossi, *Nat. Commun.* **3**, 1075 (2012).
- [23] S. John, *Phys. Rev. Lett.* **58**, 2486 (1987).
- [24] J. Topolancik, B. Ilic, and F. Vollmer, *Phys. Rev. Lett.* **99**, 253901 (2007).
- [25] M. Patterson, S. Hughes, S. Combrié, N.-V.-Q. Tran, A. De Rossi, R. Gabet, and Y. Jaouën, *Phys. Rev. Lett.* **102**, 253903 (2009).
- [26] L. Sapienza, H. Thyrrstrup, S. Stobbe, P. D. Garcia, S. Smolka, and P. Lodahl, *Science* **327**, 1352 (2010).
- [27] H. Thyrrstrup, S. Smolka, L. Sapienza, and P. Lodahl, *Phys. Rev. Lett.* **108**, 113901 (2012).
- [28] J. Liu, P. D. Garcia, S. Ek, N. Gregersen, T. Suhr, M. Schubert, J. Mørk, S. Stobbe, and P. Lodahl, *Nat. Nanotechnol.* **9**, 285 (2014).
- [29] L. Ramunno and S. Hughes, *Phys. Rev. B* **79**, 161303 (2009).
- [30] M. Patterson and S. Hughes, *Phys. Rev. B* **81**, 245321 (2010).
- [31] V. Savona, *Phys. Rev. B* **83**, 085301 (2011).
- [32] S. Johnson, M. L. Povinelli, M. Soljačić, A. Karalis, S. Jacobs, and J. D. Joannopoulos, *Appl. Phys. B* **81**, 283 (2005).
- [33] A. Javadi, S. Maibom, L. Sapienza, H. Thyrrstrup, P. D. García, and P. Lodahl, *Opt. Express* **22**, 30992 (2014).
- [34] S. G. Johnson, M. Ibanescu, M. A. Skorobogatiy, O. Weisberg, J. D. Joannopoulos, and Y. Fink, *Phys. Rev. E* **65**, 066611 (2002).
- [35] D. Marcuse, *Theory of Dielectric Optical Waveguides*, 1st ed. (Academic, New York, 1974), pp. 101–102.
- [36] L. C. Andreani and D. Gerace, *Phys. Status Solidi* **244**, 3528 (2007).
- [37] J. D. Jackson, *Classical Electrodynamics*, 3rd ed. (John Wiley & Sons, New York, 1999), Vol. 67, p. 841.
- [38] P. D. Garcia, A. Javadi, H. Thyrrstrup, and P. Lodahl, *Appl. Phys. Lett.* **102**, 031101 (2013).
- [39] D. P. Fussell, S. Hughes, and M. M. Dignam, *Phys. Rev. B* **78**, 144201 (2008).
- [40] V. S. C. Manga Rao and S. Hughes, *Phys. Rev. B* **75**, 205437 (2007).
- [41] P. Kristensen and S. Hughes, *ACS Photon.* **1**, 2 (2013).
- [42] K. M. Lee, P. T. Leung, and K. M. Pang, *J. Opt. Soc. Am. B* **16**, 1409 (1999).
- [43] R. C. Ge, P. T. Kristensen, J. F. Young, and S. Hughes, *New J. Phys.* **16**, 113048 (2014).
- [44] M. Patterson, S. Hughes, S. Schulz, D. M. Beggs, T. P. White, L. O’Faolain, and T. F. Krauss, *Phys. Rev. B* **80**, 195305 (2009).
- [45] We use Lumerical Solutions Inc., [www.lumerical.com](http://www.lumerical.com).
- [46] N. Le Thomas, H. Zhang, J. Jágerská, V. Zabelin, R. Houdré, I. Sagnes, and A. Talneau, *Phys. Rev. B* **80**, 125332 (2009).